

Review

Biodegradable Metal Organic Frameworks for Multimodal Imaging and Targeting Theranostics

Xiangdong Lai , Hui Jiang  and Xuemei Wang *

State Key Laboratory of Bioelectronics (Chien-Shiung Wu Lab), School of Biological Science and Medical Engineering, Southeast University, Nanjing 210096, China; ab58472416@163.com (X.L.); sungi@seu.edu.cn (H.J.)

* Correspondence: xuewang@seu.edu.cn; Tel.: +86-25-83792177

Abstract: Though there already had been notable progress in developing efficient therapeutic strategies for cancers, there still exist many requirements for significant improvement of the safety and efficiency of targeting cancer treatment. Thus, the rational design of a fully biodegradable and synergistic bioimaging and therapy system is of great significance. Metal organic framework (MOF) is an emerging class of coordination materials formed from metal ion/ion clusters nodes and organic ligand linkers. It arouses increasing interest in various areas in recent years. The unique features of adjustable composition, porous and directional structure, high specific surface areas, biocompatibility, and biodegradability make it possible for MOFs to be utilized as nano-drugs or/and nanocarriers for multimodal imaging and therapy. This review outlines recent advances in developing MOFs for multimodal treatment of cancer and discusses the prospects and challenges ahead.

Keywords: biodegradable materials; metal-organic framework; metal ion nodes; multimode imaging; theranostic nano-platforms



Citation: Lai, X.; Jiang, H.; Wang, X. Biodegradable Metal Organic Frameworks for Multimodal Imaging and Targeting Theranostics. *Biosensors* **2021**, *11*, 299. <https://doi.org/10.3390/bios11090299>

Received: 27 July 2021

Accepted: 24 August 2021

Published: 27 August 2021

Publisher's Note: MDPI stays neutral with regard to jurisdictional claims in published maps and institutional affiliations.



Copyright: © 2021 by the authors. Licensee MDPI, Basel, Switzerland. This article is an open access article distributed under the terms and conditions of the Creative Commons Attribution (CC BY) license (<https://creativecommons.org/licenses/by/4.0/>).

1. Introduction

Cancer has been a serious threat to human health [1]. The accurate therapy of cancer still needs to overcome many great difficulties [2,3]. Each therapy, such as chemotherapy (CT), chemo-dynamic therapy (CDT), radiation therapy (RT), radio-dynamic therapy (RDT), microwave thermal therapy (MTT), microwave dynamic therapy (MDT), photothermal therapy (PTT), and photodynamic therapy (PDT), has its inherent advantages and defects [4–6]. Hence, the treatment of cancers has gradually developed from the past monotherapy mode to the current multimode synergistic therapy to enhance therapeutic effects. With the rapid development of nanotechnology, the realization of multimode synergistic therapy depends largely on how to integrate multiple treatment modes into a single nano-platform rather than purely carrying out physical mixing to obtain a simple additive treatment effect. In recent years, emerging and rapidly developing MOF materials have shown enormous potential in multimodal synergistic therapy because of their unique porous structure and characteristics. MOF is a kind of organic inorganic hybrid material through coordination bonds formation between metal ion/ion clusters nodes and organic ligand linkers [7–11]. MOF characterizes by variable compositions and structures, adjustable porosity and pore sizes, high surface areas, good biocompatibility, and biodegradability [7,12,13]. Weak coordination bonds can endow MOFs with a stable but degradable structure [14–16]. Nanoscale pores and an ordered crystal structure allow MOFs to accumulate in tumor through enhanced permeability and retention effect (EPR) [17,18]. At the same time, the organic linker can be additionally functionalized for targeting cancer therapy [19,20]. Furthermore, the good dispersibility and biocompatibility of specific MOFs can ensure the biosafety of targeting treatment in vivo [21]. Adjustable composition results in controlled synthesis with different morphology, size, and chemical properties, making MOF itself a nano-drug for multimodal imaging and therapy by choosing appropriate metal nodes and organic ligands [22,23]. Moreover, the porous and ordered

structure and the high ratio surface areas are suitable for efficient loading of various cargos for multimodal imaging and therapy [24–28]. MOF-based nanomaterials were applied to fluorescence imaging (FL) [29–32], photoacoustic imaging (PAI) [33], magnetic resonance imaging (MRI) [34–36], computed tomography imaging (CTI) [37–39], photothermal imaging (PTI) [40,41] and positron emission tomography (PET) imaging [42–45]. It is worth mentioning that multimodal imaging [46–52] is beneficial for tumor diagnosis and accurate position. MOF-based heterogeneous hybridization may serve as an effective methodology for multimodal imaging and synergistic therapy. It integrates the advantages of various materials and endues the hybrid materials with whole new physicochemical properties, realizing theranostic nano-platforms through multimode imaging-guided therapy. In this review, the development of biodegradable MOFs as nano-drugs and nanocarriers for multimodal imaging and therapy in recent years will be summarized and discussed, as shown in Figure 1, and the prospects and challenges of MOFs in multimodal synergistic treatment will also be explored for promising clinic/biomedical applications.

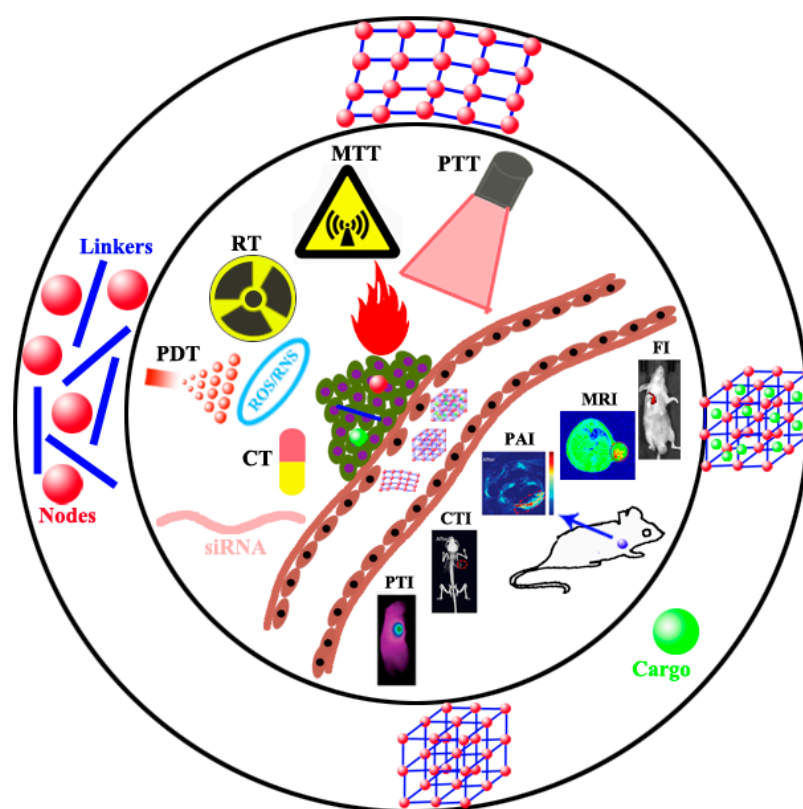


Figure 1. Schematic diagram of MOFs as nano-drugs and nanocarriers for multimodal theranostic, typically comprising a suitable and effective combination of CT, CDT, RT, RDT, PTT, PDT, MDT, MTT, gas therapy and gene therapy, and imaging of FI, MRI, PAI, CTI and PTI.

2. MOFs as Nano-Drugs

Due to the nearly infinite combination of metal ion/ion clusters nodes and organic ligand linkers, the physical and chemical properties of MOFs could be regulated for many applications. Through careful selection and design, metal ion/ion clusters nodes and organic ligand linkers can be directly and fully utilized as nano-drugs to realize multimodal imaging and therapy. Liu et al. [53] reported a nanoscale MOF synthesized by hafnium (Hf^{4+}) and tetra (4-carboxyphenyl) porphyrin (TCPP), in which TCPP as a photosensitizer converted tissue oxygen to cytotoxic singlet oxygen under light irradiation and could be used for PDT. At the same time, Hf^{4+} characterized by strong X-ray absorption capacity could act as a radiation sensitizer to enhance RT. Compared to other metals with a higher atomic number, Hf was relatively safe and showed no apparent biological

toxicity. Hf-TCPP MOF was biodegradable and easily removed from the mouse body. Hf-TCPP MOF as a biodegradable carrier-free system was used for combined RT and PDT in vitro and in vivo, demonstrating a remarkable anti-tumor effect. Lin's group [54] reported Cu-TBP (5,10,15,20-tetrabenzotoporphyrin) nanoscale MOF mediated synergistic hormone-induced CDT and light-induced PDT in the tumor model with high estradiol expression. The degradable Cu-TBP MOFs were accumulated in tumor cells efficiently and decomposed into Cu^{2+} and H_4TBP by monitoring free porphyrin fluorescence, which was entirely quenched by the paramagnetic Cu^{2+} in intact MOF at pH 7.4 and reappeared in acid tumor cell microenvironment due to the decomposition of Cu-TBP (Figure 2A). Cu-TBP was injected into dorsal subcutaneous tumors and produced Cu^{2+} and porphyrin in the low pH tumor microenvironment. Cu^{2+} ions, as redox-active metal centers, catalyzed estradiol metabolism to generate hydrogen peroxide, hydroxyl radical ($\cdot\text{OH}$), superoxide (O_2^-) species, and other ROS for CDT, whereas H_4TBP mediated light-induced PDT. This MOF-mediated radical treatment depleted intratumoral estradiol and inhibited tumor growth. Upon light irradiation, H_4TBP produced ROS to destroy the irradiated cancer cells, causing immunogenic cell death and tumor antigens release. Released tumor antigens and injected PD-L1 antibody caused the effective T cell proliferation and infiltration into the tumor, overcoming the immunosuppressive tumor microenvironment and simultaneously effectively inhibiting the growth of distant tumors (Figure 2B).

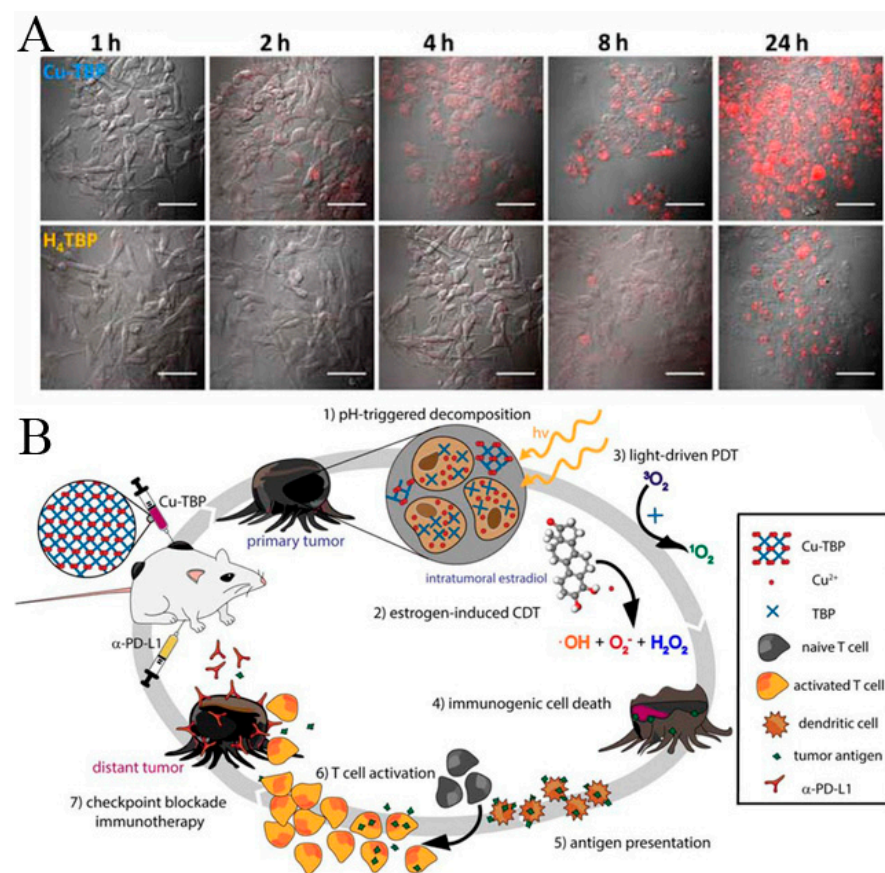


Figure 2. (A) B16F10 cellular uptake of Cu-TBP or H_4TBP at different time-points after incubation with equivalent TBP concentrations of 20 mM observed by confocal imaging. Free H_4TBP emits red fluorescence. Scale bar, 50 μm . (B) Synergy of Cu-TBP mediated radical therapy stimulated by hormone, light and checkpoint blockade immunotherapy. Reprinted with permission from Ref. [54]. Copyright 2019, Elsevier.

Zirconium(IV) chloride (ZrCl_4), Manganese(II) chloride tetrahydrate, and 1,4-Benzenedicarboxylic acid (H_2BDC) were used as raw materials to chemically synthesize Mn-doped

Zr MOF by a one-pot hydrothermal method [55]. The flexible and microporous structure is beneficial to the strongly confined inelastic collision of ions, resulting in a significant microwave thermal conversion efficiency as high as 28.7%. The Mn-ZrMOF catalyzed the degradation of H_2O_2 to generate $\cdot\text{OH}$ under MW irradiation. The *in vitro* and *in vivo* experimental studies confirmed that a union of MTT and MDT with simultaneous generation of heat and ROS under mild MW irradiation realized synergistic inhibition of the growth of tumors, as schematically reported in Figure 3. The Mn-ZrMOF was degradable *in vivo* and excreted out of the body gradually, demonstrating that it is a bio-safe therapeutic nano-agent.

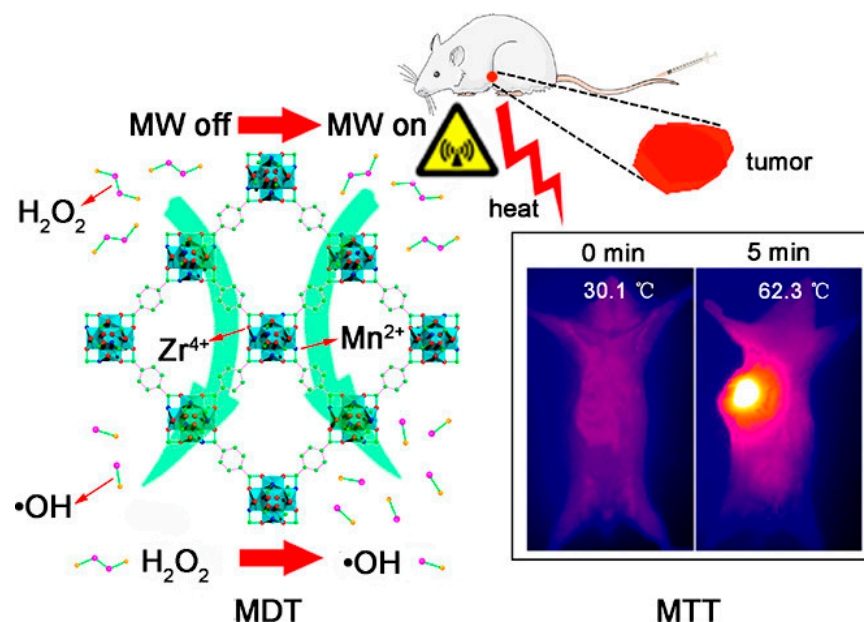


Figure 3. Mn-Zr MOF generates abundant ROS of $\cdot\text{OH}$ and a high microwave thermal conversion efficiency after exposure to MW irradiation, resulting in efficiently inhibiting the cancerous cell growth through the synergic effect of MDT and MTT. Reprinted with permission from Ref. [55]. Copyright 2018, American Chemical Society.

Lan et al. [56] reported two MOF nanolayers, $\text{Hf}_{12}\text{-Ir}$, and $\text{Hf}_6\text{-Ir}$ (namely Iridium), schematically reported in Figure 4. Under X-ray irradiation, electron-dense Hf_{12} and Hf_6 secondary building units not only generated $\cdot\text{OH}$ to enhance RT but also transferred energy to photosensitizing Ir (2,2'-bipyridine) [2-(2,4-difluorophenyl)-5-(trifluoromethyl)pyridine]₂⁺ to generate single oxygen ($^1\text{O}_2$) and O_2^- , resulting in RDT. RT and RDT exerted superb anticancer effects at shallow X-ray doses.

Wu et al. prepared Cu-TCPP MOF nanosheets for dual-modal PTT and PDT. Upon 808 nm laser irradiation, the coexisting Cu^+ and Cu^{2+} exhibited excellent photothermal performance due to the strong near-infrared (NIR) absorption [41]. In the meantime, TCPP produced $^1\text{O}_2$ for PDT. The toxicity experiment indicated that Cu-TCPP has good biocompatibility. Due to Cu(II) in the Cu-TCPP nanosheets, near-infrared thermal imaging and T1-weighted magnetic resonance imaging (MRI) could be used to realize simultaneous diagnosis and therapy (Figure 5).

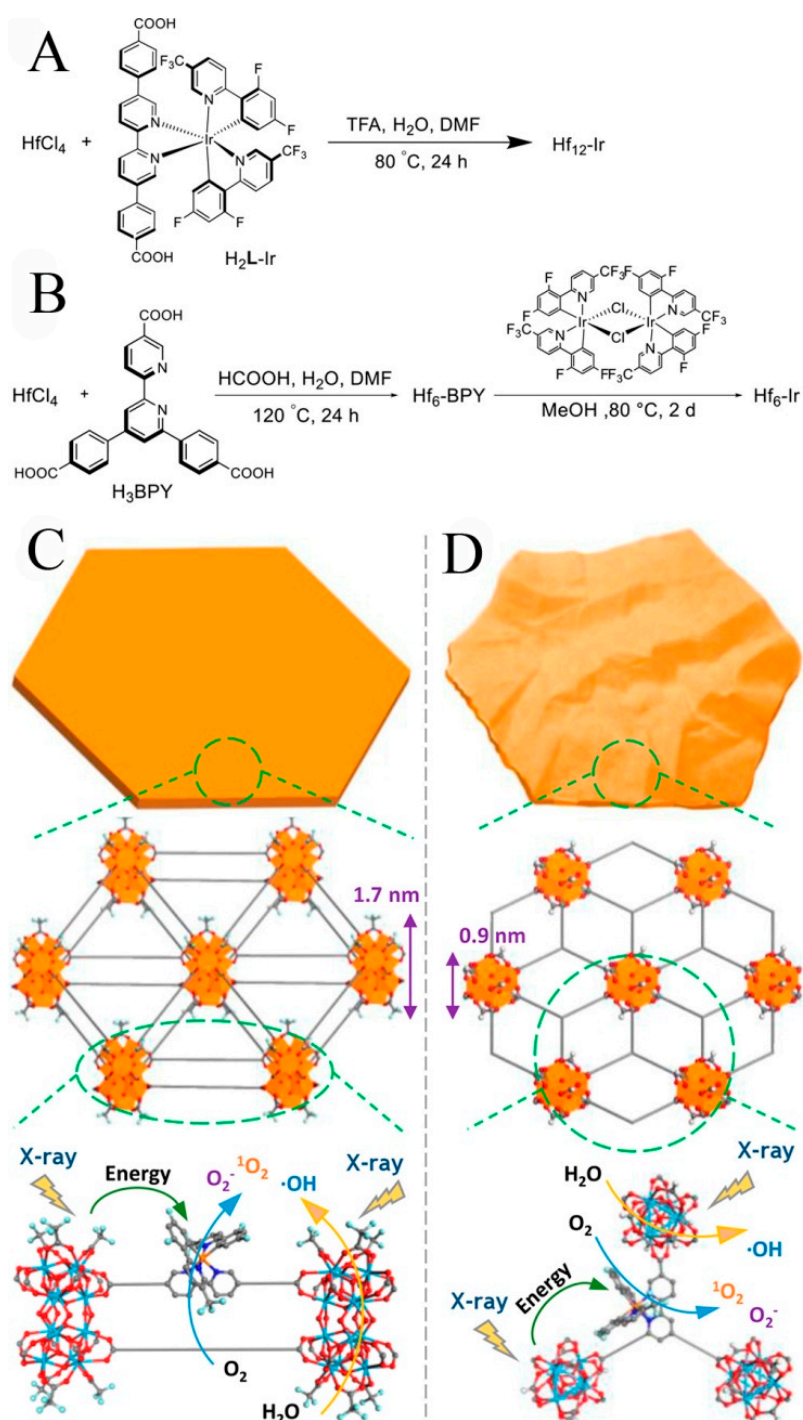


Figure 4. The synthesis methods, morphologies and structures of $\text{Hf}_{12}\text{-Ir}$ MOF nanolayer (**A,C**) and $\text{Hf}_6\text{-Ir}$ MOF nanolayer (**B,D**) and X-ray induced ROS generation. Reprinted with permission from Ref. [56]. Copyright 2018, American Chemical Society.

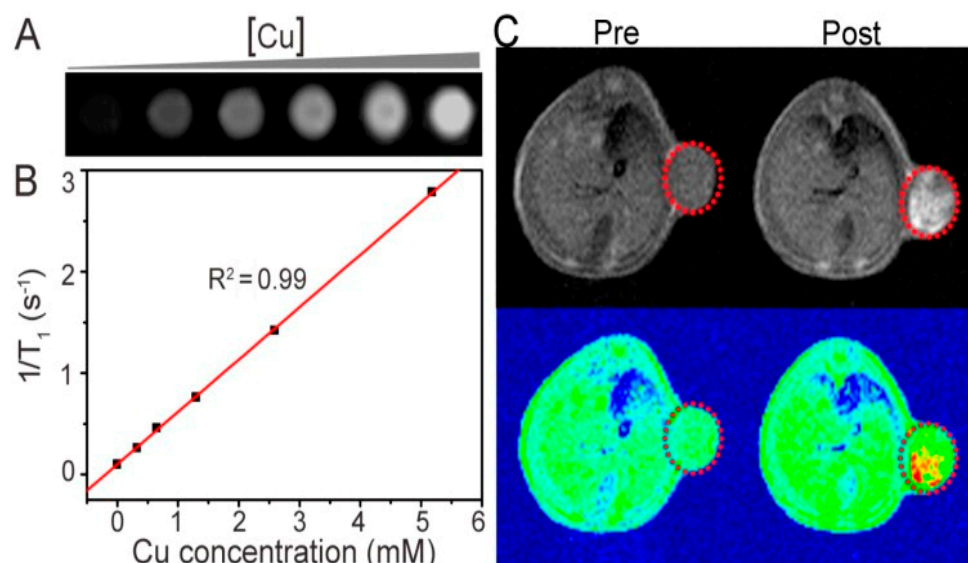


Figure 5. (A) MRI of the Cu-TCPP aqueous solution with different concentrations. (B) Plots of the $1/T_1$ value of the Cu-TCPP under concentration dependence. (C) mouse MRI before and after intratumoral injection of the Cu-TCPP. Red circles indicate the position of the tumor. Reprinted with permission from Ref. [41]. Copyright 2018, Ivyspring International Publisher.

3. MOFs as Nanocarriers

The porous and ordered structure, tunable sizes, and the high ratio surface areas make MOF easy to be loaded a variety of cargos efficiently and increase the cargo capacity. In 2006, Patricia first reported a MOF for drug delivery named Materials of Institute Lavoisier 100 and 101 (MIL-100 and 101) [57]. After more than ten years of rapid development, MOF was used to carry oxygen [58], chemotherapeutic agents [59], photosensitizer [60], photothermal conversion agents [15,61], Nucleic acids and proteins [62–65]. Du et al. [66] reported an intelligent stimuli-responsive and completely degradable MOF delivery system. Based on a “framework exchange” strategy, black phosphorous quantum dots (BPQDs) were embedded into ZIF-8 nanoparticles, which were used as sacrificial templates to prepare BP@HKUST-1 (BH). MIL-100(Fe) shell enveloped the BH core to form the core-shell structure, while *s*-nitroso-glutathione was encapsulated into HKUST-1@MIL-100. In tumor cells, the high levels of glutathione and ROS triggered the decomposition of *s*-nitroso-glutathione to produce NO and \cdot OH, causing the damage of mitochondria and DNA in tumor cells. Black phosphorus has superb biocompatibility and very high photothermal conversion efficiency. This MOF was fluorescent and photoacoustically active (Figure 6), allowing it to readily achieve accurate multiple therapies that use gas, free radicals, and PTT. Notably, this nanosystem completely degraded into phosphate radicals, terephthalic acid, and metal ions excreted out of the body.

He et al. fabricated a MOF consisting of Zr^{6+} nodes and TCPP ligand [67]. The gold nanoparticles (AuNPs) were decorated on the surface of MOF, which was conducive to effectively stabilize the nanostructure and increased radiotherapy sensitivity. Meanwhile, chemotherapeutic drug doxorubicin (Dox) was encapsulated into the MOF. The fabricated MOFs were densely packed polyethylene glycol (PEG) corona to form Dox@MOF-Au-PEG. Dox@MOF-Au-PEG oxygenated tumor microenvironment by catalyzing the degradation of H_2O_2 in tumor into O_2 , resulting in enhancing O_2 -dependent radiotherapy. Dox@MOF-Au-PEG combined the radiotherapy sensitization effect of AuNPs and the anticancer effect of Dox, achieving synergistic chemoradiotherapy, as shown in Figure 7. The stronger coordination interaction between phosphate ion and zirconium made the MOF readily decompose in PBS (2 mM), resulting in the burst release of porphyrin ligands and structural collapse. Once MOF was internalized by cancer cells, the phosphate in high concentration led to the disassembly of the NPs.

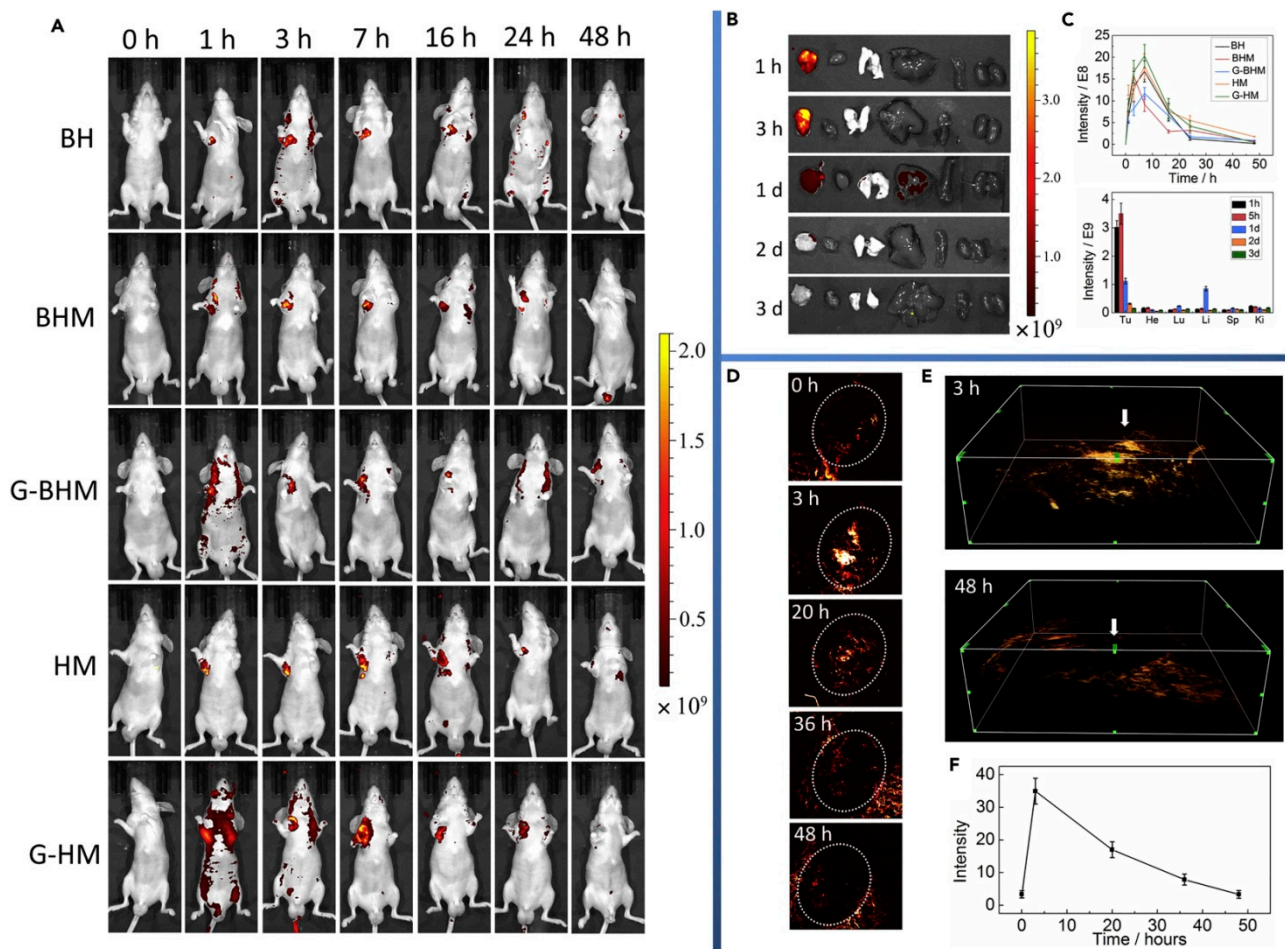


Figure 6. (A) Fluorescence imaging of SGC-7901 tumor-bearing model mice after intravenous injection of different materials at 7 time points. Unit of scale bar: $(\text{p/s/cm}^2/\text{sr})/(\text{mW/cm}^2)$. (B) Ex vivo Fluorescence imaging of tumor, heart, lung, liver, spleen, and kidney in sequence in SGC-7901 tumor-bearing model mice after intravenous injection of G-BHM at 5 different time points. (C) Time-dependent in vivo integrated FL intensity for different materials (top) and in different organs (bottom). (D) PA imaging of SGC-7901 tumor after injection of G-BHM at different time points. (E) Stereoscopic PA images, and white arrow represents tumor zone. (F) PA signal intensity variation corresponding to part (D). Reprinted with permission from Ref. [66]. Copyright 2019, Elsevier Inc.

Zhang et al. [46] prepared a porous zirconium-ferriporphyrin MOF nano-shuttles (Zr-FeP) made from $\text{ZrOCl}_2 \cdot 8\text{H}_2\text{O}$ and $\text{H}_4\text{TBP-Fe}$, carrying the siRNA of 70 kDa heat shock protein (HSP70). Under NIR lasers, the siRNA/Zr-FeP MOF catalyzed endogenous H_2O_2 and O_2 to become $\cdot\text{OH}$ and $^1\text{O}_2$, while it had high photothermal conversion efficiency up to around 34%. Moreover, siRNA reversed the HSP70-mediated chemotherapy resistance, achieving PTT at a lower-temperature and avoiding the nearby normal tissues from the nonspecific thermal radiation damage. The siRNA/Zr-FeP significantly suppressed the tumor cell growth in vitro and in vivo through the synergistic effect of PTT at a lower temperature and PDT, shown in Figure 8. siRNA/Zr-FeP was effectively cleared out of the organism, via its gradual decomposition into small molecules and ions. Meanwhile, MOF nano-shuttles achieved PAI, CTI, and photothermal imaging (PTI) tri-mode tumor-specific imaging capability, providing a powerful theranostic tool for tumors.

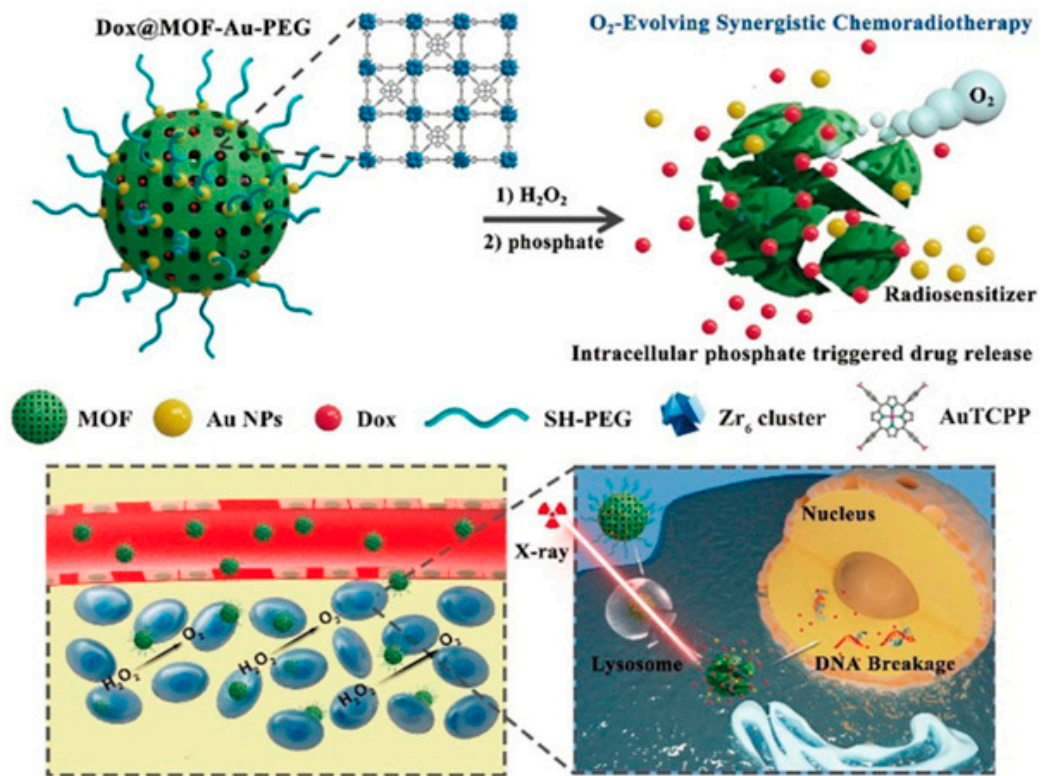


Figure 7. The structure of Dox@MOF-Au-PEG and the underlying of O₂-generating synergistic chemoradiotherapy Reprinted with permission from Ref. [67]. Copyright 2019, Wiley-VCH Verlag GmbH & Co. KGaA, Weinheim.

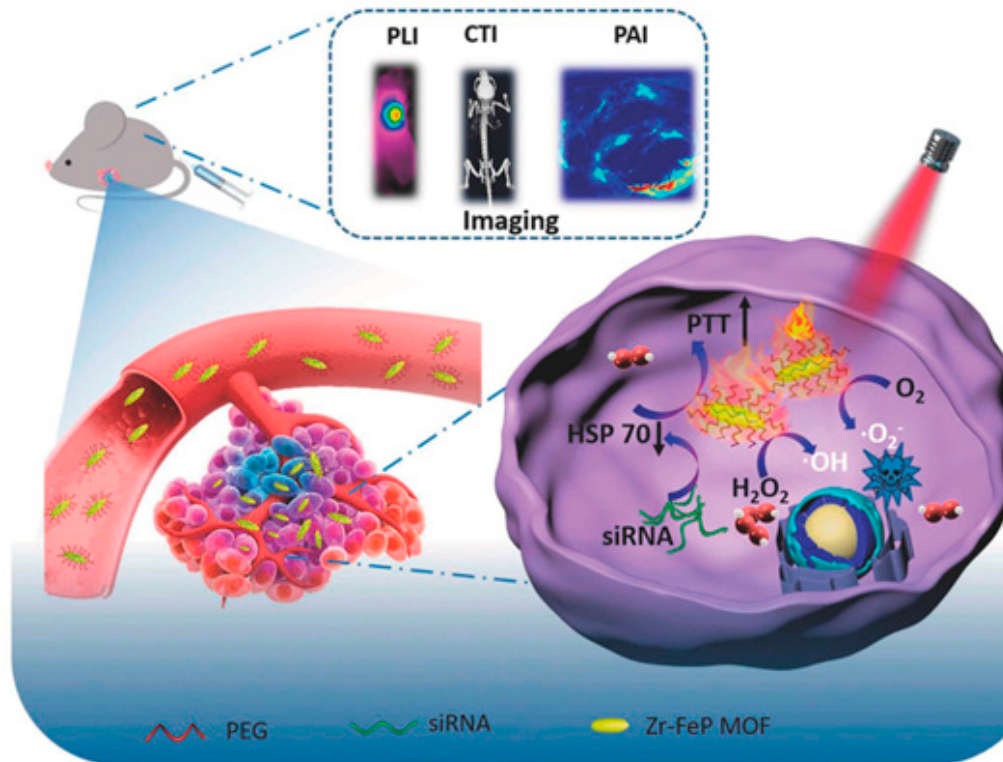


Figure 8. siRNA/Zr-FeP MOF mediates PTT at a lower temperature and PDT for cancer. Reprinted with permission from Ref. [46]. Copyright 2018, Elsevier B.V.

Liu et al. [68] encapsulated BPQDs and catalase into MIL-101 inner and outer layers, respectively, and constructed a MOF heterostructure, BPQDs-MIL@catalase-MIL. BPQDs exhibited two abilities of photothermal conversion for PTT and $^1\text{O}_2$ production for PDT. The catalase in the outer layer catalyzed H_2O_2 into O_2 . O_2 was then converted into $^1\text{O}_2$ by BPQDs in the inner layer. The PDT/PTT synergistic therapy accelerated cancer cell apoptosis. Ni et al. [69] reported a Hf-DBB-Ru MOF consisting of Hf^{4+} and bis(2,2'-bipyridine) [5,5'-di(4-benzoate)-2,2'-bipyridine] ruthenium chloride for mitochondrial-targeted RDT and RT. Ru endowed Hf-DBB-Ru with strong mitochondria-targeted ability. Hf clusters generated abundant $\cdot\text{OH}$, and Ru-based linkers produced $^1\text{O}_2$ at low dose X-ray irradiation with high penetration. Yang et al. [70] developed cypate@MIL-53 nanoparticles. Fe^{3+} metal ions and the carboxyl group of cypate interacted to form precursor complexes, improving bioavailability and protecting the cypate NIR dye from photobleaching. Organic linkers H_2BDC coordinated with Fe^{3+} to generate crystallized MOFs. PEG and transferrin were functionalized on the surface of cypate@MIL-53 to enhance biocompatibility and tumor targeted functions. Cypate molecules gave this MOF the ability to behave as photosensitizers and photothermal agents for PDT and PTT, as shown in Figure 9. This MOF realized tumor targeted multimodal imaging (Near-infrared fluorescence images, PAI, and MRI).

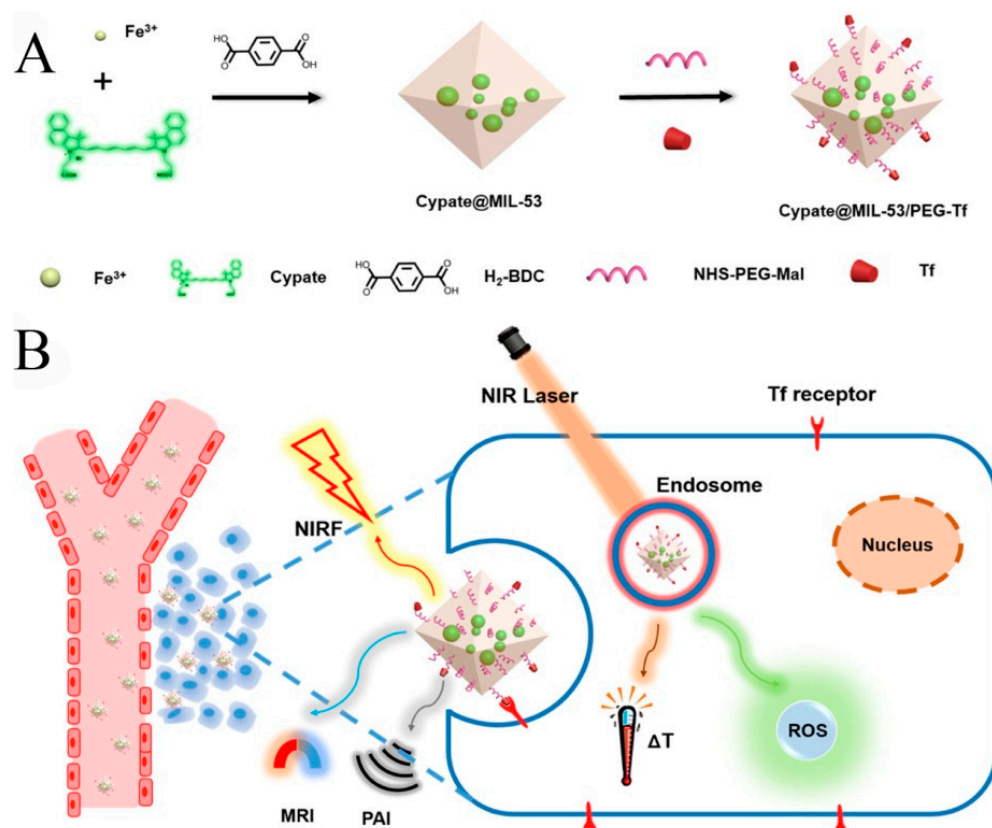


Figure 9. (A) the preparation of Cypate@MIL-53/PEG-Transferrin MOF composite and (B) its bioapplication for PDT and PTT. Reprinted with permission from Ref. [70]. Copyright 2019, American Chemical Society.

Chen et al. synthesized MIL-100 (Fe) coated Mn-based Prussian blue (PB) analogue ($\text{K}_2\text{Mn}[\text{Fe}(\text{CN})_6]$), named as PBAM, by simply stirring and heating, losing photothermal activity of PB and T1-weighted MRI due to local confinement of Mn^{2+} [20]. In the mildly acidic tumor microenvironment, the MIL-100 shell was degraded, and the released Fe^{3+} exchanged with Mn^{2+} to synthesize in situ the more stable PB, $\text{Fe}^{3+}-[\text{Fe}(\text{CN})_6]^{4-}$, and to release free Mn^{2+} . Mn^{2+} reacted with endogenous H_2O_2 and HCO_3^- and generated $\cdot\text{OH}$

for CDT. The excellent PAI and PTT of PB, and T1-weighted MRI and CDT of Mn^{2+} showed accurate theranostic effects (Figure 10).

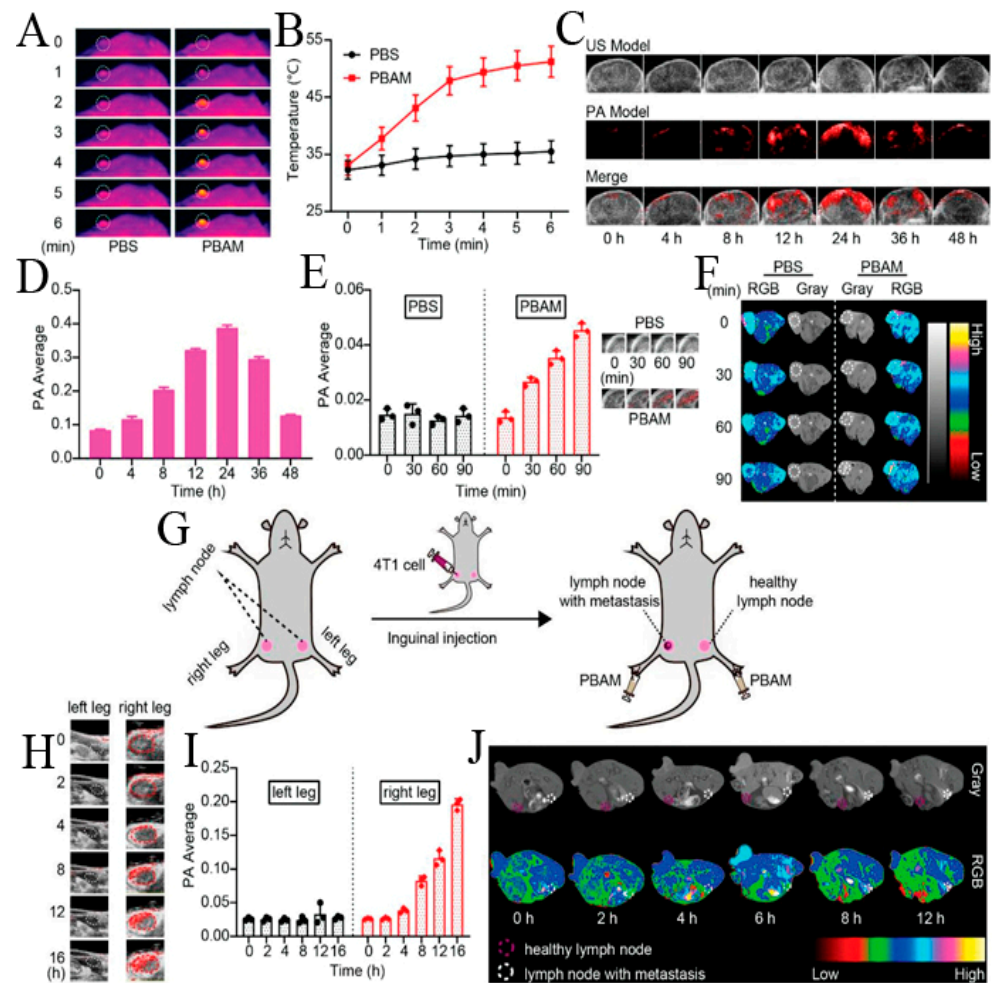


Figure 10. (A) Infrared thermal imaging and (B) tumor temperature of 4T1-tumor model mice after intravenous injection with PBAM under 808 nm laser (1 W cm^{-2}). White circle: tumor tissue. (C) Tumor PAI and (D) Corresponding PAI signal intensity of 4T1-tumor model mice after intravenous injection with PBAM. (E) Tumor PA signal intensity and corresponding PAI of 4T1-tumor model mice after subcutaneous injection with PBAM. (F) MRI of 4T1-tumor model mice after subcutaneous injection with PBAM. White circle: tumor tissue. (G) Schematic of lymphatic metastasis tumor model. (H) PAI of lymph nodes with or without metastasis at different time points after injection with PBAM. White circle: the lymph nodes in left leg. Red circle: the lymph nodes in right leg. (I) Corresponding PAI signal intensity of lymph nodes with or without metastasis. (J) MRI of lymph nodes with or without metastasis at different time points after injection with PBAM. Reprinted with permission from Ref. [20]. Copyright 2020, WILEY-VCH Verlag GmbH & Co. KGaA, Weinheim.

4. Summary and Perspectives

Weak coordination bonds result in degradable structures, which is very good for biomedical applications of MOFs. Furthermore, it is of great significance to develop MOFs as nano-drugs for multimodal imaging and therapy. MOFs itself as nano-drugs characterize by simplicity and efficiency, high drug loading, and lower dosages of node and linker drugs, benefiting for achieving expected anti-tumor effects and reducing toxic effects on normal tissues and cells. MOF specific features, such as flexible and diversified morphologies, tunable sizes, high surface areas, and tunable pore diameter make MOFs intelligent nanocarriers for multimodal diagnosis and therapy, easy to be loaded with a

variety of cargos efficiently and harbor increased cargo capacity. To sum up, we have reviewed in detail the recent progress of biodegradable MOFs for multimodal theranostic, typically comprising a suitable and effective combination of CT, CDT, RT, RDT, PTT, PDT, MDT, MTT, gas therapy, and gene therapy, and imaging of FI, MRI, PAI, CTI, and PTI.

The efficacy of single modal therapy is often not ideal due to multidrug resistance, nonspecific heating, hypoxia, and other serious adverse effects. Though MOFs for multimodal therapy have demonstrated synergistic and enhanced therapeutic efficacy and low cytotoxicity in laboratory research, there is still great room for improvements to realize targeted cancer therapy. Firstly, most excellent researches lacked long-term experiments on the toxicity of MOFs. Comprehensive studies on the absorption, biodistribution, metabolism, excretion, clearance, and long-term tissue accumulation of MOFs are necessary for determining toxicity in vivo. Toxicity is effectively prevented through choosing highly biocompatible metal ions as nodes (e.g., Ca, Fe, Zn, etc.) and endogenous bioactive molecules as ligands [71,72]. The additional loaded cargo needs to be considered as well because of probable threats to the organism. In addition, there is an ever growing need for extensive and in-depth research on the mechanisms and pathways of MOFs degradation in vivo. This is due to the fact that current single imaging methods are not sufficient to monitor and recognize the degradation process of MOFs. Finally, current studies mainly focused on dual-modal therapy [73–77], while very few reports on tri- or more modal therapies were based on MOFs, demonstrating a more effective therapy. In brief, despite facing these challenges, a significant effort has been made to develop biodegradable MOFs for multimodal imaging and therapy, which can realize clinical translations and other bio-applications in the future.

Author Contributions: Conceptualization, X.L., H.J. and X.W.; writing—original draft preparation, X.L., H.J. and X.W.; writing—review and editing, X.L., H.J. and X.W.; visualization, X.L., H.J. and X.W.; supervision, X.W.; funding acquisition, X.W. All authors have read and agreed to the published version of the manuscript.

Funding: This work was supported by the National Natural Science Foundation of China (82061148012, 82027806, 91753106), the National Key Research and Development Program of China (2017YFA0205300), and Primary Research & Development Plan of Jiangsu Province (BE2019716).

Institutional Review Board Statement: Not applicable.

Informed Consent Statement: Not applicable.

Data Availability Statement: Not applicable.

Conflicts of Interest: The authors declare no conflict of interest.

References

1. Allmani, C.; Matsuda, T.; Di Carlo, V.; Harewood, R.; Matz, M.; Niksic, M.; Bonaventure, A.; Valkov, M.; Johnson, C.J.; Esteve, J.; et al. Global surveillance of trends in cancer survival 2000–14 (CONCORD-3): Analysis of individual records for 37 513 025 patients diagnosed with one of 18 cancers from 322 population-based registries in 71 countries. *Lancet* **2018**, *391*, 1023–1075. [[CrossRef](#)]
2. Li, S.; Jiang, Q.; Liu, S.; Zhang, Y.; Tian, Y.; Song, C.; Wang, J.; Zou, Y.; Anderson, G.J.; Han, J.Y.; et al. A DNA nanorobot functions as a cancer therapeutic in response to a molecular trigger in vivo. *Nat. Biotechnol.* **2018**, *36*, 258–264. [[CrossRef](#)]
3. Cho, K.; Wang, X.; Nie, S.; Chen, Z.; Shin, D.M. Therapeutic Nanoparticles for Drug Delivery in Cancer. *Clin. Cancer Res.* **2008**, *14*, 1310. [[CrossRef](#)]
4. Goel, S.; Ferreira, C.A.; Chen, F.; Ellison, P.A.; Siamof, C.M.; Barnhart, T.E.; Cai, W. Activatable Hybrid Nanotheranostics for Tetramodal Imaging and Synergistic Photothermal/Photodynamic Therapy. *Adv. Mater.* **2018**, *30*, 1704367. [[CrossRef](#)]
5. Wang, H.; Agarwal, P.; Zhao, G.; Ji, G.; Jewell, C.M.; Fisher, J.P.; Lu, X.; He, X. Overcoming Ovarian Cancer Drug Resistance with a Cold Responsive Nanomaterial. *ACS Cent. Sci.* **2018**, *4*, 567–581. [[CrossRef](#)]
6. Zhu, Y.X.; Jia, H.R.; Pan, G.Y.; Ulrich, N.W.; Chen, Z.; Wu, F.G. Development of a Light-Controlled Nanoplatform for Direct Nuclear Delivery of Molecular and Nanoscale Materials. *J. Am. Chem. Soc.* **2018**, *140*, 4062–4070. [[CrossRef](#)]
7. Wuttke, S.; Lismont, M.; Escudero, A.; Rungtaweeworanit, B.; Parak, W.J. Positioning metal-organic framework nanoparticles within the context of drug delivery—A comparison with mesoporous silica nanoparticles and dendrimers. *Biomaterials* **2017**, *123*, 172–183. [[CrossRef](#)]

8. Chen, W.; Wu, C. Synthesis, functionalization, and applications of metal–organic frameworks in biomedicine. *Dalton Trans.* **2018**, *47*, 2114–2133. [[CrossRef](#)] [[PubMed](#)]
9. Kirchon, A.; Feng, L.; Drake, H.F.; Joseph, E.A.; Zhou, H.C. From fundamentals to applications: A toolbox for robust and multifunctional MOF materials. *Chem. Soc. Rev.* **2018**, *47*, 8611–8638. [[CrossRef](#)] [[PubMed](#)]
10. Kitagawa, S.; Kitaura, R.; Noro, S. Functional Porous Coordination Polymers. *Angew. Chem. Int. Ed.* **2004**, *43*, 2334–2375. [[CrossRef](#)] [[PubMed](#)]
11. Lee, J.; Farha, O.K.; Roberts, J.; Scheidt, K.A.; Nguyen, S.T.; Hupp, J.T. Metal–organic framework materials as catalysts. *Chem. Soc. Rev.* **2009**, *38*, 1450–1459. [[CrossRef](#)]
12. Liu, Y.; Zhao, Y.; Chen, X. Bioengineering of Metal-organic Frameworks for Nanomedicine. *Theranostics* **2019**, *9*, 3122–3133. [[CrossRef](#)]
13. Dong, Z.; Sun, Y.; Chu, J.; Zhang, X.; Deng, H. Multivariate Metal–Organic Frameworks for Dialing-in the Binding and Programming the Release of Drug Molecules. *J. Am. Chem. Soc.* **2017**, *139*, 14209–14216. [[CrossRef](#)]
14. Chen, Y.; Li, P.; Modica, J.A.; Drout, R.J.; Farha, O.K. Acid-Resistant Mesoporous Metal–Organic Framework toward Oral Insulin Delivery: Protein Encapsulation, Protection, and Release. *J. Am. Chem. Soc.* **2018**, *140*, 5678–5681. [[CrossRef](#)]
15. Wu, Q.; Niu, M.; Chen, X.; Tan, L.; Fu, C.; Ren, X.; Ren, J.; Li, L.; Xu, K.; Zhong, H.; et al. Biocompatible and biodegradable zeolitic imidazolate framework/polydopamine nanocarriers for dual stimulus triggered tumor thermo-chemotherapy. *Biomaterials* **2018**, *162*, 132–143. [[CrossRef](#)]
16. Yuan, S.; Feng, L.; Wang, K.; Pang, J.; Bosch, M.; Lollar, C.; Sun, Y.; Qin, J.; Yang, X.; Zhang, P.; et al. Stable Metal–Organic Frameworks: Design, Synthesis, and Applications. *Adv. Mater.* **2018**, *30*, e1704303. [[CrossRef](#)]
17. He, C.; Liu, D.; Lin, W. Nanomedicine Applications of Hybrid Nanomaterials Built from Metal–Ligand Coordination Bonds: Nanoscale Metal–Organic Frameworks and Nanoscale Coordination Polymers. *Chem. Rev.* **2015**, *115*, 11079–11108. [[CrossRef](#)]
18. Prabhakar, U.; Maeda, H.; Jain, R.K.; Sevcik-Muraca, E.M.; Zamboni, W.; Farokhzad, O.C.; Barry, S.T.; Gabizon, A.; Grodzinski, P.; Blakey, D.C. Challenges and key considerations of the enhanced permeability and retention effect for nanomedicine drug delivery in oncology. *Cancer Res.* **2013**, *73*, 2412–2417. [[CrossRef](#)]
19. Wang, X.G.; Xu, L.; Li, M.J.; Zhang, X.Z. Construction of Flexible-on-Rigid Hybrid-Phase Metal–Organic Frameworks for Controllable Multi-Drug Delivery. *Angew. Chem. Int. Ed.* **2020**, *59*, 18078–18086. [[CrossRef](#)] [[PubMed](#)]
20. Chen, Y.; Li, Z.H.; Pan, P.; Hu, J.J.; Cheng, S.X.; Zhang, X.Z. Tumor-Microenvironment-Triggered Ion Exchange of a Metal–Organic Framework Hybrid for Multimodal Imaging and Synergistic Therapy of Tumors. *Adv. Mater.* **2020**, *32*, e2001452. [[CrossRef](#)] [[PubMed](#)]
21. Peng, S.; Bie, B.; Sun, Y.; Liu, M.; Cong, H.; Zhou, W.; Xia, Y.; Tang, H.; Deng, H.; Zhou, X. Metal-organic frameworks for precise inclusion of single-stranded DNA and transfection in immune cells. *Nat. Commun.* **2018**, *9*, 1293. [[CrossRef](#)]
22. Lu, K.; He, C.; Lin, W. Nanoscale metal–organic framework for highly effective photodynamic therapy of resistant head and neck cancer. *J. Am. Chem. Soc.* **2014**, *136*, 16712–16715. [[CrossRef](#)]
23. Lu, K.; He, C.; Lin, W. A Chlorin-Based Nanoscale Metal–Organic Framework for Photodynamic Therapy of Colon Cancers. *J. Am. Chem. Soc.* **2015**, *137*, 7600–7603. [[CrossRef](#)]
24. Roder, R.; Preiss, T.; Hirschle, P.; Steinborn, B.; Zimpel, A.; Hohn, M.; Radler, J.O.; Bein, T.; Wagner, E.; Wuttke, S.; et al. Multifunctional Nanoparticles by Coordinative Self-Assembly of His-Tagged Units with Metal–Organic Frameworks. *J. Am. Chem. Soc.* **2017**, *139*, 2359–2368. [[CrossRef](#)]
25. Alsaiari, S.K.; Patil, S.; Alyami, M.; Alamoudi, K.O.; Aleisa, F.A.; Merzaban, J.S.; Li, M.; Khashab, N.M. Endosomal Escape and Delivery of CRISPR/Cas9 Genome Editing Machinery Enabled by Nanoscale Zeolitic Imidazolate Framework. *J. Am. Chem. Soc.* **2017**, *140*, 143–146. [[CrossRef](#)]
26. Zhao, M.; Yuan, K.; Wang, Y.; Li, G.; Guo, J.; Gu, L.; Hu, W.; Zhao, H.; Tang, Z. Metal–organic frameworks as selectivity regulators for hydrogenation reactions. *Nature* **2016**, *539*, 76–80. [[CrossRef](#)]
27. Horcajada, P.; Chalati, T.; Serre, C.; Gillet, B.; Sebrie, C.; Baati, T.; Eubank, J.F.; Heurtaux, D.; Clayette, P.; Kreuz, C.; et al. Porous metal–organic-framework nanoscale carriers as a potential platform for drug delivery and imaging. *Nat. Mater.* **2009**, *9*, 172–178. [[CrossRef](#)]
28. Zheng, H.; Zhang, Y.; Liu, L.; Wan, W.; Guo, P.; Nystrom, A.M.; Zou, X. One-pot Synthesis of Metal–Organic Frameworks with Encapsulated Target Molecules and Their Applications for Controlled Drug Delivery. *J. Am. Chem. Soc.* **2016**, *138*, 962–968. [[CrossRef](#)]
29. Wan, S.-S.; Cheng, Q.; Zeng, X.; Zhang, X.-Z. A Mn(III)-Sealed Metal–Organic Framework Nanosystem for Redox-Unlocked Tumor Theranostics. *ACS Nano* **2019**, *13*, 6561–6571. [[CrossRef](#)]
30. Zeng, J.-Y.; Zhang, M.-K.; Peng, M.-Y.; Gong, D.; Zhang, X.-Z. Porphyrinic Metal-Organic Frameworks Coated Gold Nanorods as a Versatile Nanoplatform for Combined Photodynamic/Photothermal/Chemotherapy of Tumor. *Adv. Funct. Mater.* **2018**, *28*, 1705451. [[CrossRef](#)]
31. He, Z.; Dai, Y.; Li, X.; Guo, D.; Liu, Y.; Huang, X.; Jiang, J.; Wang, S.; Zhu, G.; Zhang, F.; et al. Hybrid Nanomedicine Fabricated from Photosensitizer-Terminated Metal–Organic Framework Nanoparticles for Photodynamic Therapy and Hypoxia-Activated Cascade Chemotherapy. *Small* **2019**, *15*, e1804131. [[CrossRef](#)]
32. Yang, C.; Chen, K.; Chen, M.; Hu, X.; Huan, S.-Y.; Chen, L.; Song, G.; Zhang, X.-B. Nanoscale Metal–Organic Framework Based Two-Photon Sensing Platform for Bioimaging in Live Tissue. *Anal. Chem.* **2019**, *91*, 2727–2733. [[CrossRef](#)]

33. Zhang, K.; Yu, Z.; Meng, X.; Zhao, W.; Shi, Z.; Yang, Z.; Dong, H.; Zhang, X. A Bacteriochlorin-Based Metal–Organic Framework Nanosheet Superoxide Radical Generator for Photoacoustic Imaging-Guided Highly Efficient Photodynamic Therapy. *Adv. Sci.* **2019**, *6*, 1900530. [[CrossRef](#)]
34. Yin, S.-Y.; Song, G.; Yang, Y.; Zhao, Y.; Wang, P.; Zhu, L.-M.; Yin, X.; Zhang, X.-B. Persistent Regulation of Tumor Microenvironment via Circulating Catalysis of MnFe₂O₄@Metal–Organic Frameworks for Enhanced Photodynamic Therapy. *Adv. Funct. Mater.* **2019**, *29*, 1901417. [[CrossRef](#)]
35. Zhang, D.; Ye, Z.; Wei, L.; Luo, H.; Xiao, L. Cell Membrane-Coated Porphyrin Metal–Organic Frameworks for Cancer Cell Targeting and O₂-Evolving Photodynamic Therapy. *ACS Appl. Mater. Interfaces* **2019**, *11*, 39594–39602. [[CrossRef](#)]
36. Tian, X.-T.; Cao, P.-P.; Zhang, H.; Li, Y.-H.; Yin, X.-B. GSH-activated MRI-guided enhanced photodynamic- and chemo-combination therapy with a MnO₂-coated porphyrin metal organic framework. *Chem. Commun.* **2019**, *55*, 6241–6244. [[CrossRef](#)]
37. Liu, M.; Wang, L.; Zheng, X.; Liu, S.; Xie, Z. Hypoxia-Triggered Nanoscale Metal–Organic Frameworks for Enhanced Anticancer Activity. *ACS Appl. Mater. Interfaces* **2018**, *10*, 24638–24647. [[CrossRef](#)]
38. Liu, J.; Yang, G.; Zhu, W.; Dong, Z.; Yang, Y.; Chao, Y.; Liu, Z. Light-controlled drug release from singlet-oxygen sensitive nanoscale coordination polymers enabling cancer combination therapy. *Biomaterials* **2017**, *146*, 40–48. [[CrossRef](#)]
39. Robison, L.; Zhang, L.; Drout, R.J.; Li, P.; Haney, C.R.; Brikha, A.; Noh, H.; Mehdi, B.L.; Browning, N.D.; Dravid, V.P.; et al. A Bismuth Metal–Organic Framework as a Contrast Agent for X-ray Computed Tomography. *ACS Appl. Bio Mater.* **2019**, *2*, 1197–1203. [[CrossRef](#)]
40. Hu, X.; Lu, Y.; Zhou, L.; Chen, L.; Yao, T.; Liang, S.; Han, J.; Dong, C.; Shi, S. Post-synthesis strategy to integrate porphyrinic metal–organic frameworks with CuS NPs for synergistic enhanced photo-therapy. *J. Mater. Chem. B* **2020**, *8*, 935–944. [[CrossRef](#)]
41. Li, B.; Wang, X.; Chen, L.; Zhou, Y.; Dang, W.; Chang, J.; Wu, C. Ultrathin Cu-TCPP MOF nanosheets: A new theragnostic nanoplatform with magnetic resonance/near-infrared thermal imaging for synergistic phototherapy of cancers. *Theranostics* **2018**, *8*, 4086–4096. [[CrossRef](#)] [[PubMed](#)]
42. Zhang, Z.; Sang, W.; Xie, L.; Dai, Y. Metal-organic frameworks for multimodal bioimaging and synergistic cancer chemotherapy. *Coord. Chem. Rev.* **2019**, *399*, 213022. [[CrossRef](#)]
43. Chowdhury, M.A. Metal-Organic-Frameworks as Contrast Agents in Magnetic Resonance Imaging. *ChemBioEng Rev.* **2017**, *4*, 225–239. [[CrossRef](#)]
44. Della Rocca, J.; Liu, D.; Lin, W. Nanoscale Metal–Organic Frameworks for Biomedical Imaging and Drug Delivery. *Accounts Chem. Res.* **2011**, *44*, 957–968. [[CrossRef](#)]
45. Chen, D.; Yang, D.; Dougherty, C.A.; Lu, W.; Wu, H.; He, X.; Cai, T.; Van Dort, M.E.; Ross, B.D.; Hong, H. In Vivo Targeting and Positron Emission Tomography Imaging of Tumor with Intrinsically Radioactive Metal–Organic Frameworks Nanomaterials. *ACS Nano* **2017**, *11*, 4315–4327. [[CrossRef](#)]
46. Zhang, K.; Meng, X.; Cao, Y.; Yang, Z.; Dong, H.; Zhang, Y.; Lu, H.; Shi, Z.; Zhang, X. Metal-Organic Framework Nanoshuttle for Synergistic Photodynamic and Low-Temperature Photothermal Therapy. *Adv. Funct. Mater.* **2018**, *28*, 1804634. [[CrossRef](#)]
47. Qin, Y.-T.; Peng, H.; He, X.-W.; Li, W.-Y.; Zhang, Y.-K. pH-Responsive Polymer-Stabilized ZIF-8 Nanocomposites for Fluorescence and Magnetic Resonance Dual-Modal Imaging-Guided Chemo-/Photodynamic Combinational Cancer Therapy. *ACS Appl. Mater. Interfaces* **2019**, *11*, 34268–34281. [[CrossRef](#)] [[PubMed](#)]
48. Wang, Y.; Pang, X.; Wang, J.; Cheng, Y.; Song, Y.; Sun, Q.; You, Q.; Tan, F.; Li, J.; Li, N. Magnetically-targeted and near infrared fluorescence/magnetic resonance/photoacoustic imaging-guided combinational anti-tumor phototherapy based on polydopamine-capped magnetic Prussian blue nanoparticles. *J. Mater. Chem. B* **2018**, *6*, 2460–2473. [[CrossRef](#)]
49. Du, T.; Zhao, C.; ur Rehman, F.; Lai, L.; Li, X.; Sun, Y.; Luo, S.; Jiang, H.; Gu, N.; Selke, M.; et al. In Situ Multimodality Imaging of Cancerous Cells Based on a Selective Performance of Fe²⁺-Adsorbed Zeolitic Imidazolate Framework-8. *Adv. Funct. Mater.* **2016**, *27*, 1603926. [[CrossRef](#)]
50. Shang, W.; Zeng, C.; Du, Y.; Hui, H.; Liang, X.; Chi, C.; Wang, K.; Wang, Z.; Tian, J. Core-Shell Gold Nanorod@Metal-Organic Framework Nanoprobes for Multimodality Diagnosis of Glioma. *Adv. Mater.* **2017**, *29*, 1604381. [[CrossRef](#)]
51. Cai, W.; Gao, H.; Chu, C.; Wang, X.; Wang, J.; Zhang, P.; Lin, G.; Li, W.; Liu, G.; Chen, X. Engineering Phototheranostic Nanoscale Metal–Organic Frameworks for Multimodal Imaging-Guided Cancer Therapy. *ACS Appl. Mater. Interfaces* **2017**, *9*, 2040–2051. [[CrossRef](#)] [[PubMed](#)]
52. Zhang, H.; Shang, Y.; Li, Y.-H.; Sun, S.-K.; Yin, X.-B. Smart Metal–Organic Framework-Based Nanoplatforms for Imaging-Guided Precise Chemotherapy. *ACS Appl. Mater. Interfaces* **2019**, *11*, 1886–1895. [[CrossRef](#)]
53. Liu, J.; Yang, Y.; Zhu, W.; Yi, X.; Dong, Z.; Xu, X.; Chen, M.; Yang, K.; Lu, G.; Jiang, L.; et al. Nanoscale metal–organic frameworks for combined photodynamic & radiation therapy in cancer treatment. *Biomaterials* **2016**, *97*, 1–9. [[CrossRef](#)] [[PubMed](#)]
54. Ni, K.; Aung, T.; Li, S.; Fatuzzo, N.; Liang, X.; Lin, W. Nanoscale Metal-Organic Framework Mediates Radical Therapy to Enhance Cancer Immunotherapy. *Chem* **2019**, *5*, 1892–1913. [[CrossRef](#)]
55. Fu, C.; Zhou, H.; Tan, L.; Huang, Z.; Wu, Q.; Ren, X.; Ren, J.; Meng, X. Microwave-Activated Mn-Doped Zirconium Metal–Organic Framework Nanocubes for Highly Effective Combination of Microwave Dynamic and Thermal Therapies Against Cancer. *ACS Nano* **2018**, *12*, 2201–2210. [[CrossRef](#)]
56. Lan, G.; Ni, K.; Veroneau, S.S.; Song, Y.; Lin, W. Nanoscale Metal–Organic Layers for Radiotherapy–Radiodynamic Therapy. *J. Am. Chem. Soc.* **2018**, *140*, 16971–16975. [[CrossRef](#)]

57. Horcajada, P.; Serre, C.; Vallet-Regi, M.; Sebban, M.; Taulelle, F.; Ferey, G. Metal–organic frameworks as efficient materials for drug delivery. *Angew. Chem. Int. Ed.* **2006**, *45*, 5974–5978. [[CrossRef](#)]
58. Gao, S.; Zheng, P.; Li, Z.; Feng, X.; Yan, W.; Chen, S.; Guo, W.; Liu, D.; Yang, X.; Wang, S.; et al. Biomimetic O₂-Evolving metal-organic framework nanoplatfor platform for highly efficient photodynamic therapy against hypoxic tumor. *Biomaterials* **2018**, *178*, 83–94. [[CrossRef](#)]
59. Ling, D.; Li, H.; Xi, W.; Wang, Z.; Bednarkiewicz, A.; Dibaba, S.T.; Shi, L.; Sun, L. Heterodimers made of metal–organic frameworks and upconversion nanoparticles for bioimaging and pH-responsive dual-drug delivery. *J. Mater. Chem. B* **2020**, *8*, 1316–1325. [[CrossRef](#)]
60. Meng, X.; Deng, J.; Liu, F.; Guo, T.; Liu, M.; Dai, P.; Fan, A.; Wang, Z.; Zhao, Y. Triggered All-Active Metal Organic Framework: Ferroptosis Machinery Contributes to the Apoptotic Photodynamic Antitumor Therapy. *Nano Lett.* **2019**, *19*, 7866–7876. [[CrossRef](#)]
61. Zhang, L.; Li, S.; Chen, X.; Wang, T.; Li, L.; Su, Z.; Wang, C. Tailored Surfaces on 2D Material: UFO-Like Cyclodextrin-Pd Nanosheet/Metal Organic Framework Janus Nanoparticles for Synergistic Cancer Therapy. *Adv. Funct. Mater.* **2018**, *28*, 1803815. [[CrossRef](#)]
62. Zheng, D.-W.; Lei, Q.; Zhu, J.-Y.; Fan, J.-X.; Li, C.-X.; Li, C.; Xu, Z.; Cheng, S.-X.; Zhang, X.-Z. Switching Apoptosis to Ferroptosis: Metal–Organic Network for High-Efficiency Anticancer Therapy. *Nano Lett.* **2017**, *17*, 284–291. [[CrossRef](#)]
63. Zhang, Y.; Lin, L.; Liu, L.; Liu, F.; Sheng, S.; Tian, H.; Chen, X. Positive feedback nanoamplifier responded to tumor microenvironments for self-enhanced tumor imaging and therapy. *Biomaterials* **2019**, *216*, 119255. [[CrossRef](#)] [[PubMed](#)]
64. Li, Y.; Zhang, K.; Liu, P.; Chen, M.; Zhong, Y.; Ye, Q.; Wei, M.Q.; Zhao, H.; Tang, Z. Encapsulation of Plasmid DNA by Nanoscale Metal–Organic Frameworks for Efficient Gene Transportation and Expression. *Adv. Mater.* **2019**, *31*, e1901570. [[CrossRef](#)] [[PubMed](#)]
65. Alyami, M.Z.; Alsaiari, S.K.; Li, Y.; Qutub, S.S.; Aleisa, F.A.; Sougrat, R.; Merzaban, J.S.; Khashab, N.M. Cell-Type-Specific CRISPR/Cas9 Delivery by Biomimetic Metal Organic Frameworks. *J. Am. Chem. Soc.* **2020**, *142*, 1715–1720. [[CrossRef](#)]
66. Du, T.; Qin, Z.; Zheng, Y.; Jiang, H.; Weizmann, Y.; Wang, X. The “Framework Exchange”-Strategy-Based MOF Platform for Biodegradable Multimodal Therapy. *Chem* **2019**, *5*, 2942–2954. [[CrossRef](#)]
67. He, Z.; Huang, X.; Wang, C.; Li, X.; Liu, Y.; Zhou, Z.; Wang, S.; Zhang, F.; Wang, Z.; Jacobson, O.; et al. A Catalase-Like Metal–Organic Framework Nanohybrid for O₂-Evolving Synergistic Chemoradiotherapy. *Angew. Chem. Int. Ed.* **2019**, *58*, 8752–8756. [[CrossRef](#)]
68. Liu, J.; Liu, T.; Du, P.; Zhang, L.; Lei, J. Metal–Organic Framework (MOF) Hybrid as a Tandem Catalyst for Enhanced Therapy against Hypoxic Tumor Cells. *Angew. Chem. Int. Ed.* **2019**, *58*, 7808–7812. [[CrossRef](#)]
69. Ni, K.; Lan, G.; Veroneau, S.S.; Duan, X.; Song, Y.; Lin, W. Nanoscale metal-organic frameworks for mitochondria-targeted radiotherapy-radiodynamic therapy. *Nat. Commun.* **2018**, *9*, 4321. [[CrossRef](#)]
70. Yang, P.; Men, Y.; Tian, Y.; Cao, Y.; Zhang, L.; Yao, X.; Yang, W. Metal–Organic Framework Nanoparticles with Near-Infrared Dye for Multimodal Imaging and Guided Phototherapy. *ACS Appl. Mater. Interfaces* **2019**, *11*, 11209–11219. [[CrossRef](#)]
71. Giménez-Marqués, M.; Hidalgo, T.; Serre, C.; Horcajada, P. Nanostructured metal–organic frameworks and their bio-related applications. *Coord. Chem. Rev.* **2016**, *307*, 342–360. [[CrossRef](#)]
72. Simon-Yarza, T.; Mielcarek, A.; Couvreur, P.; Serre, C. Nanoparticles of Metal-Organic Frameworks: On the Road to In Vivo Efficacy in Biomedicine. *Adv. Mater.* **2018**, *30*, e1707365. [[CrossRef](#)] [[PubMed](#)]
73. Guo, H.; Yi, S.; Feng, K.; Xia, Y.; Qu, X.; Wan, F.; Chen, L.; Zhang, C. In situ formation of metal organic framework onto gold nanorods/mesoporous silica with functional integration for targeted theranostics. *Chem. Eng. J.* **2021**, *403*, 126432. [[CrossRef](#)]
74. Ma, Y.; Chen, L.; Li, X.; Hu, A.; Wang, H.; Zhou, H.; Tian, B.; Dong, J. Rationally Integrating Peptide-induced targeting and multimodal therapies in a dual-shell theranostic platform for orthotopic metastatic spinal tumors. *Biomaterials* **2021**, *275*, 120917. [[CrossRef](#)] [[PubMed](#)]
75. Zou, M.; Zhao, Y.; Ding, B.; Jiang, F.; Chen, Y.; Ma, P.; Lin, J. NIR-triggered biodegradable MOF-coated upconversion nanoparticles for synergetic chemodynamic/photodynamic therapy with enhanced efficacy. *Inorg. Chem. Front.* **2021**, *8*, 2624–2633. [[CrossRef](#)]
76. Meng, X.; Zhang, K.; Yang, F.; Dai, W.; Lu, H.; Dong, H.; Zhang, X. Biodegradable Metal–Organic Frameworks Power DNzyme for in Vivo Temporal-Spatial Control Fluorescence Imaging of Aberrant MicroRNA and Hypoxic Tumor. *Anal. Chem.* **2020**, *92*, 8333–8339. [[CrossRef](#)] [[PubMed](#)]
77. Cai, X.; Xie, Z.; Ding, B.; Shao, S.; Liang, S.; Pang, M.; Lin, J. Monodispersed Copper(I)-Based Nano Metal–Organic Framework as a Biodegradable Drug Carrier with Enhanced Photodynamic Therapy Efficacy. *Adv. Sci.* **2019**, *6*, 1900848. [[CrossRef](#)]